analytical chemistry

Article

Cite This: Anal. Chem. 2019, 91, 12352−12357

pubs.acs.org/ac

Dark-Field Microscopic Detection of Bacteria using Bacteriophage-Immobilized SiO_2@AuNP Core−Shell Nanoparticles

Masashi Imai,[†] Kouhei Mine,[‡] Haruna Tomonari,[§] Jumpei Uchiyama,[#] Shigenobu Matuzaki,[⊥] Yosuke Niko,[∥] Shingo Hadano,[∥] and Shigeru Watanabe*[,∥]

[†]TOSA Innovative Human Development Programs, [‡]Department of Science, Faculty of Science, [§]Department of Applied Science, Faculty of Science, and [∥]Department of Chemistry and Biotechnology, Faculty of Science and Technology, Kochi University, 2-5-1 Akebono-cho, Kochi-shi 780-8520, Kochi, Japan

[#]School of Veterinary Medicine, Azabu University, 1-17-71 Fuchinobe, Sagamihara-shi 229-8501, Kanagawa, Japan

[⊥]Department of Microbiology and Infection, Kochi Medical School, Kochi University, Kohasu, Okoh-cho, Nankoku-shi 780-8505, Kochi, Japan

Supporting Information

ABSTRACT: To replace molecular biological and immunological methods, biosensors have recently been developed for the rapid and sensitive detection of bacteria. Among a wide variety of biological materials, bacteriophages have received increasing attention as promising alternatives to antibodies in biosensor applications. Thus, we herein present a rapid and highly selective detection method for pathogenic bacteria, which combines dark-field light scattering imaging with a plasmonic biosensor system. The plasmonic biosensor system employs bacteriophages as the biorecognition element and the aggregation-induced light scattering signal of gold nanoparticle-assembled silica nanospheres as a signal transducer. Using *Staphylococcus aureus* strain SA27 as a model analyte, we demonstrated that the plasmonic biosensor system detects *S. aureus* in the presence of excess *Escherichia coli* in a highly selective manner. After the sample and the *S. aureus* phage S13′-conjugated plasmon scattering probe were mixed, *S. aureus* detection was completed within 15−20 min with a detection limit of 8×10^4 colony forming units per milliliter.

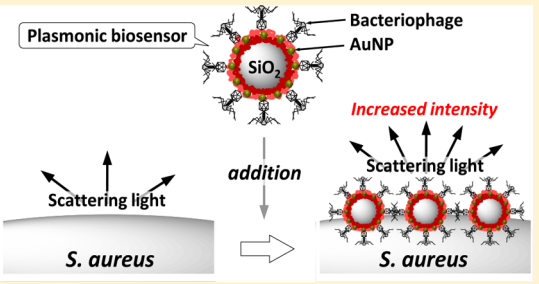

Bacterial infections are a serious worldwide threat to public health, and so the accurate and rapid detection and identification of pathogenic bacteria are of particular importance not only in the context of public health but also for medical diagnoses, food safety, environmental monitoring, and anti-bioterrorism purposes.[1,2] However, traditional culture-based methods, although cheap and straightforward, are laborious, time-consuming, and only suitable for viable and cultivable cells. In recent years, numerous culture-independent techniques have been developed for the rapid and sensitive detection of pathogenic bacteria. Among them, molecular biological (DNA microarray,[3] polymerase chain reaction (PCR) detection, and derivatives[4−6]) and immunological methods (enzyme-linked immunosorbent assays (ELISA),[7−9] lateral flow immunoassays,[10−12] and immunomagnetic separation[13−16]) are the most commonly employed. However, these methods require expensive equipment and highly trained laboratory analysts.[17] Furthermore, PCR is particularly sensitive to the quality of the selected primers and probes, while immunoassays are limited by the availability of antibodies with high affinities and specificities. To overcome such limitations, more recent approaches have focused on biosensors.[18,19]

More specifically, biosensors consist of a bioreceptor and a transducer that converts the recognition events mediated by bioreceptors into measurable or detectable signals.[2,18,19] The most important component for a biosensor is the bioreceptor as a biorecognition element, as this determines the selectivity of the biosensor. A variety of biological materials, including antibodies, enzymes, DNA, aptamers, and lectin, is combined with signal transducers composed of optical, electrochemical, piezoelectric, and thermal detection platforms to improve the performances of biosensors for bacterial detection.[20,21]

In recent years, bacteriophages (phages) have received increasing attention as promising alternatives to antibodies in biosensor applications.[22−25] Phages are viruses that infect only the host bacteria.[26,27] They are harmless to humans, animals, and plants, are much less expensive and faster to produce than antibodies, and have longer shelf lives. Biosensors that employ phages as bioreceptors are able to detect the majority of bacteria through infection. However, most phages tend to infect only one species or even a few strains within a species. It

Received: June 14, 2019
Accepted: August 29, 2019
Published: August 29, 2019

DOI: 10.1021/acs.analchem.9b02715
Anal. Chem. 2019, 91, 12352−12357

is therefore possible to specifically detect any existing bacteria by employing the phage specific to that particular bacterial target. Some phages are also robust and retain their detectable activity even after exposure to temperatures of 76 °C over 3 d[28] or following exposure to organic solvents.[29,30] In addition, large quantities of phages can be prepared simply by their infection of bacteria. These advantages render phages ideal bioreceptors in biosensors for rapid bacterial detection.[22,25]

Dark-field microscopy is a highly sensitive imaging technique, as it is essentially background-free, and it is significantly more cost-effective than flow cytometry or fluorescence microscopy, which employ laser or high-power white light as the light sources, respectively. In addition, gold nanoparticles (AuNPs) exhibit highly efficient light-scattering properties due to the collective oscillations of electrons on the AuNP surface caused by light, which is otherwise known as localized surface plasmon resonance (LSPR). The magnitude of light scattering by 60 nm AuNPs is 5 orders higher than the light emission from strongly fluorescing dyes,[31,32] and so the combination of these two technologies provides novel solutions that enable the rapid and sensitive detection of bacteria.[33−35]

Thus, we herein describe the rapid and selective detection of bacteria based on a combination of dark-field microscopy and phage-immobilized plasmon scattering nanoprobes. More specifically, AuNPs will be self-assembled on larger SiO_2 spheres (SiO_2@AuNP) to give a plasmon scattering nanoprobe, and the specificity of the phage-based nanoprobes toward the host bacteria will be examined.

EXPERIMENTAL SECTION

Chemicals. Hydrogen tetrachloroaurate trihydrate ($HAuCl_4 \cdot 3H_2O$) (>49.0% Au) and trisodium citrate dehydrate (>99%) were obtained from Wako Pure Chemical Industries, Ltd. and were used as received. Silica nanospheres (Seahoster KE-P30, d_{ave} = 300 nm) were obtained from Nippon Shokubai Co., Ltd., while poly(diallyl dimethylammonium chloride) (PDDA, Mw: 100 000−200 000 g mol^{-1}, 20 wt % in water) was purchased from Sigma-Aldrich. All other reagents and solvents were purchased as reagent grade from Wako Pure Chemical Industries, Ltd. or Nakalai Tesque, Inc. and were used without further purification. Ultrapure water (electric resistivity 18.2 MΩ·cm^{-1}) was obtained using a Milli-Q water purification system (Millipore Co.).

Phages, Bacteria, Cultures, and Culture Media. *Staphylococcus* virus S13′ was employed herein as previously described in the literature.[36,37] *S. aureus* strain SA27 was used as the host bacterial strain for *Staphylococcus* virus S13′, while *E. coli* strain DH5alpha was used as a negative control (Takara Bio). The phages and bacteria were cultured in LB media (LB Broth, Miller; Nacalai Tesque) at 37 °C.

Phage Amplification and Purification. The phages were purified according to a previously described technique,[38] and they were cultured using an appropriate host bacterial strain in culture media (500 mL). After phage amplification and precipitation of the cell debris, the phages were concentrated by the addition of poly(ethylene glycol) and NaCl and subsequent centrifugation. The phage suspension was then subjected to CsCl density-gradient centrifugation (40 000*g*, 2 h, 4 °C) to give a phage band, which was collected from the tube and dialyzed against ammonium acetate solution (AAS) (0.1 mol l^{-1} ammonium acetate, 10 mmol mol l^{-1} NaCl, 1 mmol l^{-1} $CaCl_2$, 1 mmol l^{-1} $MgCl_2$, pH 7.2, 4 °C, overnight). The purified phage suspension was then filtered through a 0.45 μm syringe filter, and the phage quantity was enumerated in terms of the plaque-forming units.

Instrumentation. UV−Vis measurements were performed on a double-beam Jasco V-560 UV−vis spectrophotometer (Jasco Ltd.) at 298 K, using 1 cm path length quartz cuvettes. Dynamic light scattering (DLS) experiments were conducted using a DLS-6000 light scattering spectrometer (Photal Otsuka Electronics Co., Ltd.). Incident light was provided by a He−Ne laser (λ_{ex} = 632.8 nm) operating at 10 mW. Scattering light was collected at a fixed angle of 90°. The ζ potentials of the prepared nanoparticles were measured using an ELSZ-2 ζ potential analyzer (Otsuka Electronics). All field-emission scanning electron microscopy (FE-SEM) images were acquired using a JEOL JSM-6500F instrument equipped with a cold-field emission gun and a semi-in-lens secondary electron detector. For all measurements, the accelerating voltage was 1.0 kV, and the emission current was 1.0 μA. All transmission electron microscopy (TEM) measurements were performed on a Hitachi H-7110 transmission electron microscope at an accelerating voltage of 100 kV. The TEM samples were prepared by dropping a solution of the nanoparticles onto amorphous carbon-coated Cu grids (Okenshoji Co., Ltd., No. 10-1012: Elastic carbon ELS-C10, STEM Cu100P grid) and dried for 2 h at 35 °C. The grids were then exposed to RuO_4 vapor (0.5% aqueous solution) for 4 h at 25 °C prior to drying under air overnight. Fluorescence images were acquired with an AxioObserverZ1 fluorescence microscope equipped with a 4′,6-diamidino-2-phenylindole (DAPI) filter set (Zeiss filter set 49; excitation G 365, dichroic FT 395, emission BP 445/50) (Zeiss). Dark-field images were acquired using an inverted Zeiss AxioObserverZ1 microscope. A 100 W halogen lamp was focused on the sample using a high numerical immersion condenser (numerical aperture (NA) = 1.4), and the scattered light was collected by an EC Plan-Neofluar 100× objective (NA = 0.7, Zeiss). Color images were acquired using a Canon X9 color CMOS camera (Canon Inc.) connected to one of the microscope eyepieces.

Synthesis of the SiO_2@AuNP Core−Shell Nanoparticles. Silica nanospheres were added to water (1.5 mL) in a test tube and subjected to ultrasonication for 1.5 h. After this time, the resulting suspension was transferred to a 100 mL beaker and allowed to stir vigorously. To the mixing suspension was added an aqueous solution of PDDA (332 μL) and NaCl (398 mg, 6.8 mmol). After it was stirred at 25 °C for 20 min, the reaction mixture was subjected to centrifugation at 2810*g* for 20 min, and the obtained precipitate was dispersed in water (10 mL) and stored at 4 °C prior to characterization and further use.

The aqueous suspension of PDDA-modified SiO_2 (2.5 mL, 2.79×10^9 particles mL^{-1}) was added to an aqueous solution of citrate-reduced AuNPs[39] (8.0 mL, 1.0×10^3 pM, $d = 32.5 \pm 3.0$ nm). After it was vortexed for 3 min, the obtained mixture was allowed to stand for 2 h. To remove any free AuNPs, the reaction mixture was centrifuged at 700*g* for 20 min, and the resulting light brown precipitate was redispersed in water and stored at 25 °C prior to characterization and further use.

Synthesis of the Phage-Immobilized SiO_2@AuNP Core−Shell Nanoparticles. To a suspension of the SiO_2@AuNPs (5 mL) was added an aqueous solution of PDDA (166 μL) and NaCl (398 mg, 6.8 mmol). After it was stirred at 25 °C for 20 min, the reaction mixture was subjected to centrifugation at 2810*g* for 20 min, and the resulting

DOI: 10.1021/acs.analchem.9b02715
Anal. Chem. 2019, 91, 12352−12357

precipitate was resuspended in 10 mM phosphate-buffered saline (PBS) (pH 7.1, 5 mL) prior to further centrifugation at 2810*g* for 20 min. The washing step was repeated twice. To a suspension of the PDDA-coated SiO_2@AuNPs (800 μL, density of solution 6.98 × 10^8 particles mL^{-1}) was added a suspension of the phage (1 × 10^{-12} plaque-forming units mL^{-1}) in PBS buffer (240 μL), and the mixture was incubated at 4 °C. The tube was then subjected to centrifugation at 1100*g* for 20 min, after which the supernatant was removed. The resulting pellet was resuspended in 10 mM PBS (pH 7.1, 800 μL), swirled carefully, and stored at 4 °C prior to further use.

Optimization of the Mixing Ratio of the Phage-Immobilized SiO_2@AuNPs to Bacteria. To a 20 μL suspension of *S. aureus* (3.0 × 10^7 cfu mL^{-1}) in PBS buffer (pH 7.1) was added the S13′-SiO_2@AuNP suspension (40 μL, 2.4, 6.3, 12.6, 25.3, 37.9, and 50.5 × 10^8 particles mL^{-1}). After incubation at 25 °C for 3 min, the dark-field images were acquired.

Quantitative Detection. A *S. aureus* suspension of 1 × 10^9 cfu mL^{-1} was diluted serially 10-fold to give concentrations ranging from 1 × 10^8 to 1 × 10^5 cfu mL^{-1}. The 1.4 × 10^9 particle mL^{-1} suspension of the phage-immobilized SiO_2@AuNP (40 μL) was mixed with different concentrations of the *S. aureus* suspension (20 μL), vortexed, and incubated at 25 °C for 3 min. After this time, an aliquot of the resulting mixture (20 μL) was placed onto the bacterial counter and spread with a coverslip. The edges of the coverslip were sealed with fingernail polish. The bacterial counters were observed immediately using a Zeiss AxioObserverZ1 microscope equipped with an AxioCam HRm. Quantitative analysis was performed on the sampling fields for a volume of 0.13 mm^3. A direct count was then performed using two 3 mm square counting chambers (0.01 mm^3 each), and more than 10 bacteria were used to achieve accurate bacterial counting.[33]

RESULTS AND DISCUSSION

Preparation of the Phage-Immobilized SiO_2@AuNP Core−Shell Nanoparticles. AuNPs have the ability to resonantly scatter visible and near-infrared light upon excitation of their surface plasmon oscillation. AuNP aggregates in which several AuNPs are condensed in a limited volume can act as an efficient light-scattering probe on dark-field light scattering imaging. However, precise control of the size and structure of the aggregate is difficult, and so we prepared AuNPs self-assembled on larger SiO_2 spheres (SiO_2@AuNPs) as a stable, uniform, and efficient plasmon scattering nanoprobe. Using aggregated AuNPs on a spherical SiO_2 template can provide another advantage over a large AuNP. The SiO_2@AuNPs are considerably stable even in a high salt buffer desired for phage immobilization, which is enough to aggregate gold nanoparticles. As shown in Scheme 1, the SiO_2@AuNPs were prepared via a layer-by-layer self-assembly method, where following the initial coating of SiO_2 spheres (300 nm diameter) with PDDA to provide a positively charged surface (ζ = 56.4 ± 0.8 mV) that assists subsequent uniform and dense deposition of the negatively charged AuNPs, the surface charge of the SiO_2 spheres became negative (ζ = −27.3 ± 3.6 mV). Finally, PDDA was coated on the SiO_2@AuNPs to reproduce the positively charged surface. For each step, the particle suspension was subjected to repeated centrifugation/water washing cycles to remove any unadsorbed material. Successful formation of the cationic SiO_2@AuNPs was confirmed by SEM observations, UV−vis spectroscopy, ζ-potential measurements (ζ = 33.8 ± 2.2 mV), and light scattering measurements (d = 408.2 ± 8.1 nm) (Figures S1 and S2).

Scheme 1. Synthesis of the Phage-Immobilized SiO_2@AuNP Core−Shell Nanoparticles

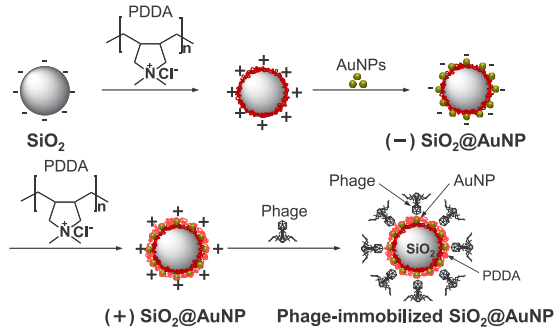

The phages were then immobilized on the surfaces of the positively charged SiO_2@AuNPs as biorecognition elements for bacterial detection (Scheme 1). The phages were considered to bind bacteria via their tail fibers, which must be free and oriented perpendicular to the surface. The majority of phages have a net negative charge with a negatively charged head and positively charged tail fibers.[40] This charge difference between the head and tail fibers of the phage could be utilized for oriented immobilization of the phages on the SiO_2@AuNPs through electrostatic interactions.[41] The positively charged SiO_2@AuNPs were then exposed to a solution of phage S13′ in PBS buffer, followed by centrifugation and washing to remove any unbound phages. The UV−vis spectrum of the phage S13′-immobilized SiO_2@AuNPs shows that the LSPR peak was red-shifted from 543.2 to 550.4 nm following phage immobilization. In addition, the ζ-potential decreased from 33.8 to −29.6 mV. The average hydrodynamic diameter of the phage S13′-immobilized SiO_2@AuNPs measured by DLS increased to 557.0 ± 1.7 nm. This increase of 74.5 nm corresponds with an average diameter of 76.8 nm for the phage S13′ as determined by DLS. Figure S3 shows bright-field and fluorescence microscopic images of the SiO_2@AuNPs modified with the DAPI-labeled phage S13′. Merging of these images clearly shows that the phages are located on the SiO_2@AuNP surfaces. Furthermore, a TEM image of the phage-immobilized SiO_2@AuNPs shows that the phages are bound to the SiO_2@AuNPs (Figure 1).

Dark-Field Images of the AuNPs, Phage-Immobilized SiO_2@AuNPs, and Bacteria. Under the dark-field micro-

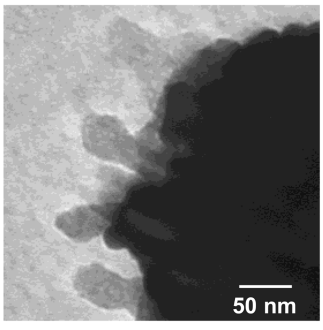

Figure 1. TEM image of the S13′ phage-immobilized SiO_2@AuNPs.

DOI: 10.1021/acs.analchem.9b02715
Anal. Chem. 2019, 91, 12352−12357

scope, the 40 nm AuNPs were difficult to observe, while the SiO_2@AuNPs and the phage-immobilized SiO_2@AuNPs were clearly visible (Figure 2), indicating that the SiO_2@AuNPs

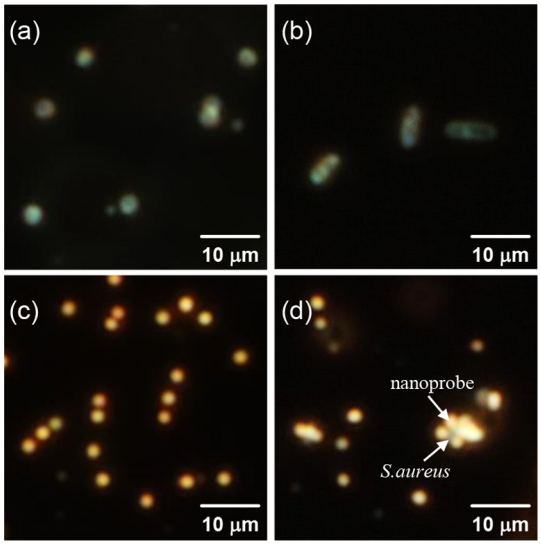

Figure 2. Dark-field images of (a) *S. aureus*, (b) *E. coli*, (c) S13′ phage-immobilized SiO_2@AuNPs, and (d) *S. aureus* labeled with S13′ phage-immobilized SiO_2@AuNPs for 3 min at 25 °C.

display excellent light-scattering properties. The scattering light color of the S13′ phage-immobilized SiO_2@AuNPs is completely different from that of *S. aureus* and *E. coli*. The former is orange, and the latter is light blue. The S13′ phage-immobilized SiO_2@AuNPs are also brighter than *S. aureus* and *E. coli*, and most importantly, the bacteria labeled with the phage-immobilized SiO_2@AuNPs are the brightest objects due to the enhanced plasmon resonance scattering light resulting from aggregation of the phage-immobilized SiO_2@AuNPs. The color of the scattering light is also informative; the labeled bacterial cells appear light blue to white with orange patches in contrast to the intrinsic light blue scattering from the unlabeled bacterial cells. These color differences can help mitigate false-positive detection due to self-aggregation of the S13′ phage-immobilized SiO_2@AuNPs, which appear orange.

Optimal Mixing Ratio of the Phage-Immobilized SiO_2@AuNPs to Bacteria. When counted under the microscope, the number of bacteria was clearly related to the concentration of the bacterial suspension employed. In addition, the dark-field imaging performance was found to be significantly dependent on the mixing ratio of the phage-immobilized SiO_2@AuNPs to the bacteria. Figure 3 shows the dependency of the light-scattering intensity on the mixing ratio of the phage-immobilized SiO_2@AuNPs to bacteria, where the bacteria mixed with the phage-immobilized SiO_2@AuNPs scattered considerably more light than the untreated bacteria. The light scattering intensity drastically increased from 20 to 100 of the mixing ratio and plateaued at ∼200 of the mixing ratio. An increase in the strength of light scattering indicates an increase in the quantity of phage-immobilized SiO_2@AuNPs bound to a bacterium. Finally, binding of the phage-immobilized SiO_2@AuNPs progresses rapidly, eventually saturating the bacterial surface.

Bacterial Selectivity of the Phage-Immobilized SiO_2@AuNPs. The bacterial selectivity of the *S. aureus* phage S13′-immobilized SiO_2@AuNPs was then evaluated by comparing

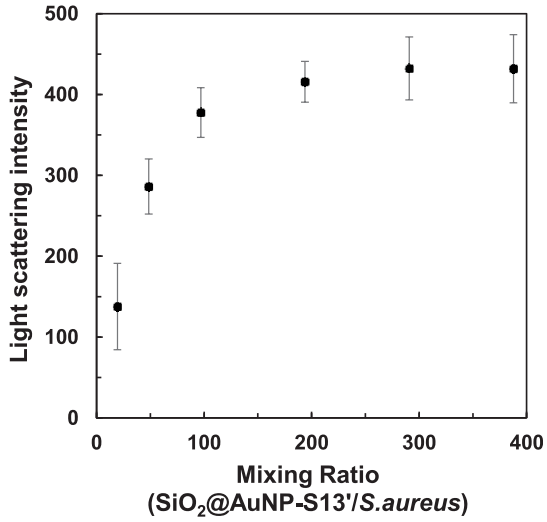

Figure 3. Dependency of the light-scattering intensity on the mixing ratio of the SiO_2@AuNP-S13′ to bacteria.

the dark-field images of a target bacterium (i.e., *S. aureus*) and a control bacterium (i.e., *E. coli*). The unmodified SiO_2@AuNPs readily adsorbed onto both bacteria in aqueous solution due to electrostatic attractions between the negatively charged bacteria and the positively charged SiO_2@AuNPs. The presence of SiO_2@AuNP-bound bacteria thereby resulted in an increase in the light-scattering intensity in the dark-field images (Figures 4e,f). Under the detection conditions, free SiO_2@AuNPs were relatively unstable, and some of them formed irregular self-aggregates, which produced orange scattering light in the dark-field images. In contrast, the S13′-immobilized SiO_2@AuNPs selectively targeted *S. aureus* and increased only the scattering contrast of *S. aureus* (Figures 4g,h). Such selective contrast enhancement results from the highly specific and selective binding of the phage S13′ to *S. aureus*. The S13′ phage-immobilized SiO_2@AuNPs bound to *S. aureus* along the shape of individual bacterial cells, which resulted in the formation of round-shaped aggregates. This can also help to distinguish between the nanoprobe-labeled bacteria and the nanoprobe self-aggregates. Furthermore, the SEM images clearly show a preference for binding to *S. aureus* over *E. coli* (Figure 5). Interestingly, the highly selective and targeted *S. aureus* imaging could be achieved even in the presence of a 15-fold excess of *E. coli* (Figure 6). Under these conditions, the phage-immobilized SiO_2@AuNPs were highly dispersible and more resistant to nonspecific self-aggregation than the unbound SiO_2@AuNPs, lowering the risk of false-positive results.

Quantitative Detection. To enable the accurate, efficient, and reproducible quantification of bacteria, the number of bacteria was counted by dark-field microscopy using a dark-field counter. The bacterial numbers were plotted against those detected by the plate-counting method (Figure 7), and the dark-field imaging results showed a good correlation with the plate counting, giving a slope of 0.88 (R^2 = 0.998) over a wide concentration range of targeted bacteria. Dark-field imaging with a plasmon scattering nanoprobe is sufficiently sensitive to detect a single bacterium. Consequently, the lower limit of detection strictly depends on the total volume observed under the microscope. Quantitative analysis was therefore performed on the sampling fields for a volume of 0.13 mm^3. A direct count was then performed using two 3 mm square counting

DOI: 10.1021/acs.analchem.9b02715
Anal. Chem. 2019, 91, 12352−12357

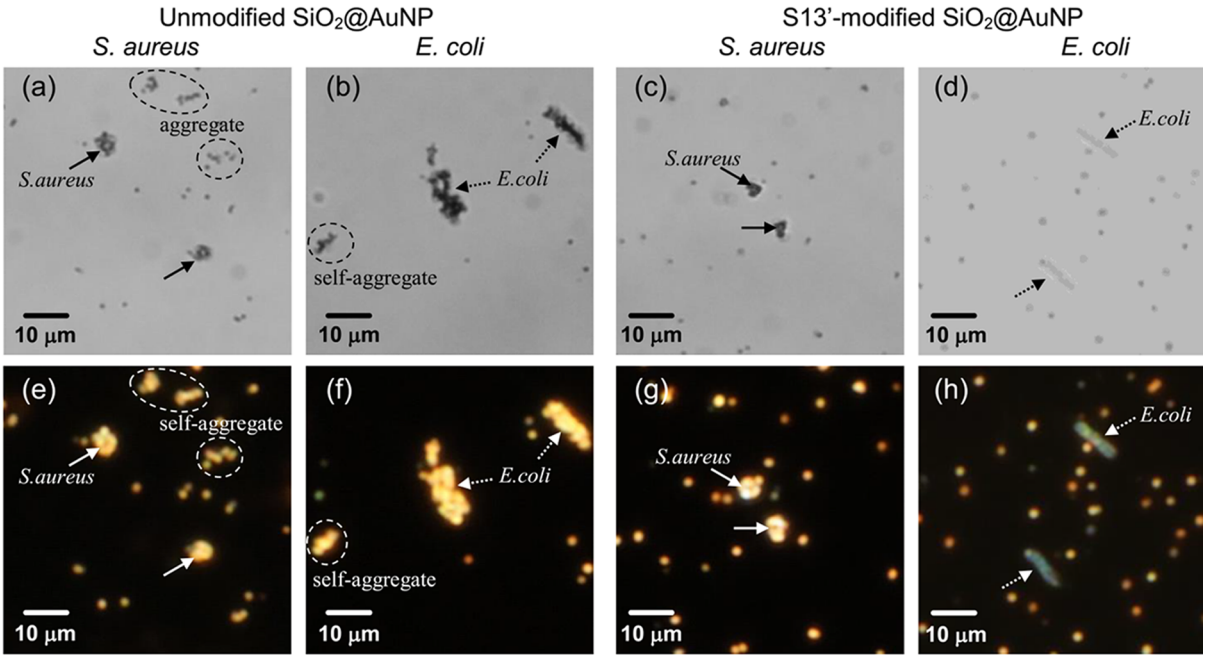

Figure 4. (a–d) Bright-field and (e–h) dark-field microscopy images of *S.aureus* and *E. coli* reacted with the unmodified and the phage S13′-modified SiO_2@AuNPs.

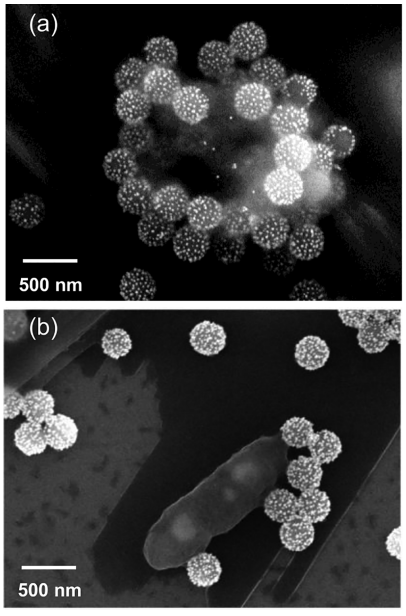

Figure 5. SEM images of (a) *S. aureus* and (b) *E. coli* reacted with the S13′-immobilized SiO_2@AuNPs.

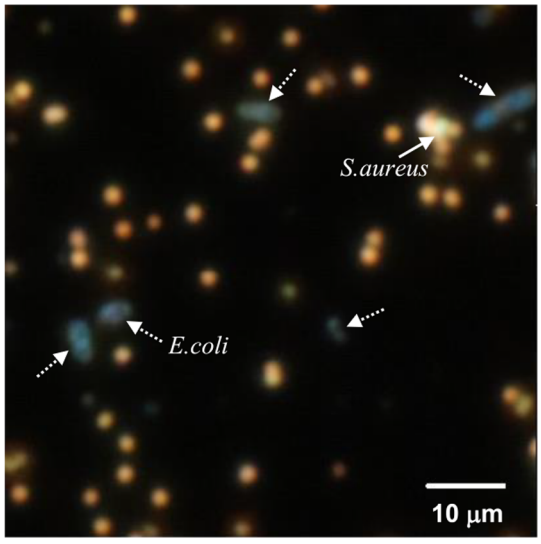

Figure 6. Dark-field image of *S. aureus* upon the addition of the phage S13′-immobilized SiO_2@AuNPs in the presence of a 15-fold excess of *E. coli* in 10 mM PBS buffer (pH 7.1) at 25 °C.

chambers (0.01 mm^3 each), and more than 10 bacteria were used to achieve accurate bacterial counting.[33] From the sampling area containing 10 bacteria, a detection limit of 8 × 10^4 cfu mL^{-1} was obtained. This is comparable to the lowest value (i.e., 1 × 10^5 cfu mL^{-1}) that can be reached by bacterial detection without any preconcentration or any enzymatic signal enhancement.

CONCLUSION

We herein demonstrated the use of phage-immobilized SiO_2@AuNP core–shell nanoparticles as a plasmon scattering probe for dark-field microscopy imaging. The phage S13′ was able to specifically recognize and bind to *S. aureus*, while the SiO_2@AuNP core–shell nanoparticles were employed to enhance the light scattering intensity of the target bacteria. The detection limit for *S. aureus* was ∼1 × 10^4 cfu mL^{-1}, and the quantification of target bacteria over a wide range of concentrations was accomplished within 15–20 min after addition of the probes to the bacterial solution. The present method therefore exhibits potential for expanding its application to the selective, sensitive, and rapid detection of any bacterium by changing the phages employed. Further studies into the detection of bacteria at concentrations less than 1 × 10^4 cfu mL^{-1} using bifunctional plasmonic-magnetic nanoparticles are now in progress in our laboratory.

DOI: 10.1021/acs.analchem.9b02715
Anal. Chem. 2019, 91, 12352–12357

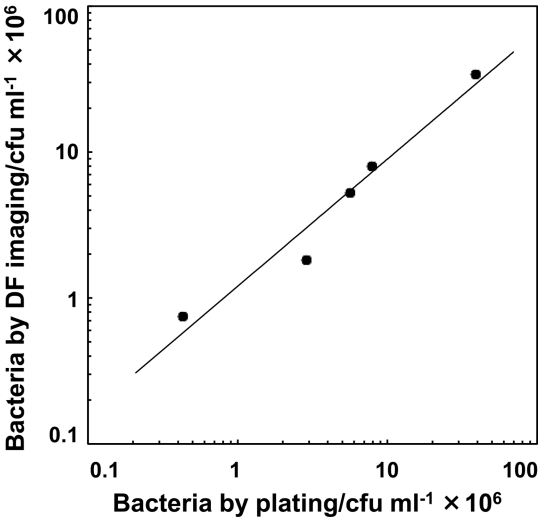

Figure 7. Calibration curve obtained from the dark-field images of *S. aureus* upon the addition of the phage S13′-immobilized SiO_2@AuNPs in 10 mM PBS buffer (pH 7.1) at 25 °C.

■ ASSOCIATED CONTENT

Supporting Information

The Supporting Information is available free of charge on the ACS Publications website at DOI: 10.1021/acs.analchem.9b02715.

SEM image, bright-field image, fluorescence image, UV−vis spectra (PDF)

■ AUTHOR INFORMATION

Corresponding Author

*Phone: +81-88-844-8301. Fax: +81-88-844-8359. E-mail: watanabe@kochi-u.ac.jp.

ORCID

Shigeru Watanabe: 0000-0003-1686-1764

Notes

The authors declare no competing financial interest.

■ ACKNOWLEDGMENTS

This work was supported by JSPS KAKENHI Grant Nos. JP15K05541 and JP18K05174.

■ REFERENCES

(1) Váradi, L.; Luo, J. L.; Hibbs, D. E.; Perry, D. J.; Anderson, J. R.; Orenga, S.; Groundwater, P. W. *Chem. Soc. Rev.* **2017**, *46*, 4818−4832.

(2) Ahmed, A.; Rushworth, J. V.; Hirst, N. A.; Millner, P. A. *Clin. Microbiol. Rev.* **2014**, *27*, 631−646.

(3) Uttamchandani, M.; Neo, J. L.; Ong, B. N. Z.; Moochhala, S. *Trends Biotechnol.* **2009**, *27*, 53−61.

(4) Liang, F.; Browne, D. J.; Gray, M. J.; Gartlan, K. H.; Smith, D. D.; Barnard, R. T.; Hill, G. R.; Corrie, S. R.; Markey, K. A. *ACS Infect. Dis.* **2018**, *4*, 837−844.

(5) Monis, P. T.; Giglio, S. *Infect., Genet. Evol.* **2006**, *6*, 2−12.

(6) Bai, J.; Baldwin, E.; Liao, H.-L.; Zhao, W.; Kostenyuk, I.; Burns, J.; Irey, M. *J. Agric. Food Chem.* **2013**, *61*, 9339−9346.

(7) Zhu, L.; He, J.; Cao, X.; Huang, K.; Luo, Y.; Xu, W. *Sci. Rep.* **2016**, *6*, 16092.

(8) Palumbo, J. D.; Borucki, M. K.; Mandrell, R. E.; Gorski, L. *J. Clin. Microbiol.* **2003**, *41*, 564−571.

(9) Albritton, H. L.; Kozlowski, P. A.; Lillis, R. A.; McGowin, C. L.; Siren, J. D.; Taylor, S. N.; Ibana, J. A.; Buckner, L. R.; Shen, L.; Quayle, A. J. *PLoS One* **2017**, *12*, e0183101.

(10) Zhang, L.; Huang, Y.; Wang, J.; Rong, Y.; Lai, W.; Zhang, J.; Chen, T. *Langmuir* **2015**, *31*, 5537−5544.

(11) Cho, I.-H.; Bhunia, A.; Irudayaraj, J. *Int. J. Food Microbiol.* **2015**, *206*, 60−66.

(12) Shan, S.; Lai, W.; Xiong, Y.; Wei, H.; Xu, H. *J. Agric. Food Chem.* **2015**, *63*, 745−753.

(13) Gu, H.; Xu, K.; Xu, C.; Xu, B. *Chem. Commun.* **2006**, 941−949.

(14) Wen, C.-Y.; Jiang, Y.-Z.; Li, X.-Y.; Tang, M.; Wu, L.-L.; Hu, J.; Pang, D.-W.; Zeng, J.-B. *ACS Appl. Mater. Interfaces* **2017**, *9*, 9416−9425.

(15) Sung, Y. J.; Suk, H.-J.; Sung, H. Y.; Li, T.; Poo, H.; Kim, M.-G. *Biosens. Bioelectron.* **2013**, *43*, 432−439.

(16) Wang, C.; Irudayaraj, J. *Small* **2010**, *6*, 283−289.

(17) Law, J. W.-F.; Ab Mutalib, N.-S.; Chan, K.-G.; Lee, L.-H. *Front. Microbiol.* **2015**, *5*, 770.

(18) Yoo, S. M.; Lee, S. Y. *Trends Biotechnol.* **2016**, *34*, 7−25.

(19) Kumar, N.; Hu, Y.; Singh, S.; Mizaikoff, B. *Analyst* **2018**, *143*, 359−373.

(20) Chen, J.; Andler, M. S.; Goddard, J. M.; Nugen, S. R.; Rotello, V. M. *Chem. Soc. Rev.* **2017**, *46*, 1272−1283.

(21) Templier, V.; Roux, A.; Roupioz, Y.; Livache, T. *TrAC, Trends Anal. Chem.* **2016**, *79*, 71−79.

(22) Richter, Ł.; Janczuk-Richter, M.; Niedziółka-Jönsson, J.; Paczesny, J.; Hołyst, R. *Drug Discovery Today* **2018**, *23*, 448−455.

(23) van der Merwe, R. G.; van Helden, P. D.; Warren, R. M.; Sampson, S. L.; Gey van Pittius, N. C. *Analyst* **2014**, *139*, 2617−2626.

(24) Tawil, N.; Sacher, E.; Mandeville, R.; Meunier, M. *Analyst* **2014**, *139*, 12124−12136.

(25) Anany, H.; Chou, Y.; Cucic, S.; Derda, R.; Evoy, S.; Griffiths, M. W. *Annu. Rev. Food Sci. Technol.* **2017**, *8*, 305−329.

(26) Salmond, G. P. C.; Fineran, P. C. *Nat. Rev. Microbiol.* **2015**, *13*, 777−786.

(27) Waldor, M. K.; Friedman, D. I.; Adhya, S. L. *Phages: Their Role in Pathogen and Biotechnology;* American Society for Microbiology Press: Washington, DC, 2005.

(28) Brigati, J. R.; Petrenko, V. A. *Anal. Bioanal. Chem.* **2005**, *382*, 1346−1350.

(29) Royston, E.; Lee, S.-Y.; Culver, J. N.; Harris, M. T. *J. Colloid Interface Sci.* **2006**, *298*, 706−712.

(30) Bruckman, M. A.; Kaur, G.; Lee, L. A.; Xie, F.; Sepulveda, J.; Breitenkamp, R.; Zhang, X.; Joralemon, M.; Russell, T. P.; Emrick, T.; Wang, Q. *ChemBioChem* **2008**, *9*, 519−523.

(31) Yguerabide, J.; Yguerabide, E. E. *Anal. Biochem.* **1998**, *262*, 137−156.

(32) Yguerabide, J.; Yguerabide, E. E. *Anal. Biochem.* **1998**, *262*, 157−176.

(33) Xu, X.; Chen, Y.; Wei, H.; Xia, B.; Liu, F.; Li, N. *Anal. Chem.* **2012**, *84*, 9721−9728.

(34) Shiigi, H.; Kinoshita, T.; Fukuda, M.; Le, D. Q.; Nishino, T.; Nagaoka, T. *Anal. Chem.* **2015**, *87*, 4042−4046.

(35) Kinoshita, T.; Kiso, K.; Le, Q. D.; Shiigi, H.; Nagaoka, T. *Anal. Sci.* **2016**, *32*, 301−305.

(36) Uchiyama, J.; Taniguchi, M.; Kurokawa, K.; Takemura-Uchiyama, I.; Ujihara, T.; Shimakura, H.; Sakaguchi, Y.; Murakami, H.; Sakaguchi, M.; Matsuzaki, S. *J. Gen. Virol.* **2017**, *98*, 2171−2180.

(37) Takemura-Uchiyama, I.; Uchiyama, J.; Kato, S.-i.; Inoue, T.; Ujihara, T.; Ohara, N.; Daibata, M.; Matsuzaki, S. *FEMS Microbiol. Lett.* **2013**, *347*, 52−60.

(38) Nasukawa, T.; Uchiyama, J.; Taharaguchi, S.; Ota, S.; Ujihara, T.; Matsuzaki, S.; Murakami, H.; Mizukami, K.; Sakaguchi, M. *Arch. Virol.* **2017**, *162*, 3523−3528.

(39) Frens, G. *Nature (London), Phys. Sci.* **1973**, *241*, 20−22.

(40) Rohwer, F.; Barott, K. *Biol. Philos.* **2013**, *28*, 283−297.

(41) Cademartiri, R.; Anany, H.; Gross, I.; Bhayani, R.; Griffiths, M.; Brook, M. A. *Biomaterials* **2010**, *31*, 1904−1910.

DOI: 10.1021/acs.analchem.9b02715
Anal. Chem. 2019, 91, 12352−12357